

Entanglement convertibility by sweeping through the phase diagram of one dimensional XXZ model with bond alternation

Yu-Chin Tzeng,^{1,*} Li Dai,^{1,*} Ming-Chiang Chung,¹ Luigi Amico,^{2,3} and Leong-Chuan Kwek^{3,4,5,6}

¹*Department of Physics, National Chung Hsing University, Taichung, Taiwan*

²*CNR-MATIS-IMM & Dipartimento di Fisica e Astronomia, Università di Catania, & INFN-Laboratori Nazionali del Sud, Via S. Sofia 64, 95127 Catania (Italy)*

³*Centre for Quantum Technologies, National University of Singapore, 3 Science Drive 2, Singapore 117543, Singapore*

⁴*Institute of Advanced Studies, Nanyang Technological University, 60 Nanyang View, Singapore 639673, Singapore*

⁵*National Institute of Education, Nanyang Technological University, 1 Nanyang Walk, Singapore 637616, Singapore*

⁶*MajuLab, CNRS-UNS-NUS-NTU International Joint Research Unit, UMI 3654, Singapore*

(Dated: February 10, 2022)

We study the entanglement structure and the topological edge states of the ground state of the spin-1/2 XXZ model with bond alternation. We employ density matrix renormalization group with periodic boundary conditions. The finite-size scaling of Rényi entropies S_2 and S_∞ are used to construct the phase diagram of the system. The phase diagram displays three possible phases: Haldane type (an example of symmetry protected topological ordered phases), dimer and Néel phases, the latter bounded by two continuous quantum phase transitions. The entanglement and non-locality in the ground state are studied by looking at the response of the ground state entanglement to a change of the control parameter. Such a response is quantified by the so called entanglement convertibility. We found that, at small spatial scales, the ground state is not convertible within the topological Haldane dimer phase. The phenomenology we observe can be described in terms of correlations between edge states. We found that the entanglement spectrum also exhibits a distinctive response in the topological phase: the effective rank of the reduced density matrix displays a specifically large 'susceptibility' in the topological phase. These findings support the idea that although the topological order in the ground state cannot be detected by local inspection, the ground state response at local scale can tell the topological phases apart from the non-topological phases.

PACS numbers: 03.67.Mn, 03.65.Vf, 75.10.Pq, 64.70.Tg

I. INTRODUCTION

Many-body quantum states are generically entangled. Consequently, considerable efforts have been made to understand the physical implications of this simple fact[1, 2]. The issue is very challenging since the entanglement found in many-body quantum states is highly multipartite, and it is distributed in a complex form[3, 4] with complicated structure[5]. Nevertheless, important results have been obtained for characterizing quantum phases of matter, or the phases of ground states, in terms of their entanglement. Aside from disordered and ordered phases characterized by a non-vanishing (local) order parameter, quantum phases with more subtle order have since been found. This is the case of spin liquids and topologically ordered ground states[6]. These phases, and the phase transitions between them, cannot be characterized within the mechanism of Landau symmetry breaking. Yet, these phases and their phase transitions exhibit patterns of long range entanglement that implies that a correlation, although tenuous, can be of global nature (respect to a local scale implied by the bare interaction)[7].

In this paper, we analyze the entanglement structure of a quantum state through the entanglement convertibility. The latter is concerned with the conversion between

quantum states through the Local Operations and Classical Communication (LOCC). This convertibility can be used to characterize the quantum entanglement of the states. The rationale for that is fairly simple: since LOCC cannot change the entanglement, the convertibility properties of the state define equivalent classes for entangled states. For bipartite pure states, meaning that the system can be divided into two subsystems A and B, the best ratio of M'/M if M copies of $|\psi_{AB}\rangle$ are converted into M' copies of $|\psi'_{AB}\rangle$ (entanglement of formation and entanglement of distillation) is provided by $S_v(\rho_A)/S_v(\rho'_A)$, where $S_v(\rho_A) = -\text{Tr}(\rho_A \ln \rho_A)$ is the von Neuman entropy of $\rho_A = \text{Tr}_B(|\psi_{AB}\rangle\langle\psi_{AB}|)$ and ρ'_A is the reduced state of the subsystem A for $|\psi'_{AB}\rangle$ [8, 9]. However, the scenario is very different when only a single copy of the state is available for converting into another single copy of the target state through LOCC. Interestingly, in this case, it is not always possible to convert a state exactly into another state with the same or lower entanglement using only LOCC. To quantify the single copy entanglement conversion, we need to go beyond the informations provided by the von Neuman entropy, and a more complete knowledge of the eigenvalues of the reduced density operator is adduced through the Entanglement Spectrum (ES) [10] or, equivalently, through the Rényi entropies which provides a re-parametrization of the ES:

$$S_\alpha(\rho_A) = \frac{1}{1-\alpha} \ln(\text{Tr}\rho_A^\alpha), \quad (1)$$

* These authors contributed equally to this work.

where $\alpha \geq 0$. The case $\alpha = 1$ corresponds to the von Neumann entropy. To the best of our knowledge, the single copy entanglement conversion cannot be expressed as a simple condition on the ES if a *catalyst* is not involved in the process of the conversion[11, 12]. The catalyst here is a bipartite state that participates in the conversion process but remains intact after the conversion is done. In such a case, the necessary and sufficient condition for the convertibility of the state $|\psi_{AB}\rangle$ into $|\psi'_{AB}\rangle$ is that $S_\alpha(\rho_A) \geq S_\alpha(\rho'_A)$ for all $\alpha \geq 0$. Whether or not the catalyst is necessary in the conversion depends on the following majorization condition. Suppose the eigenvalues of ρ_A are $(\omega_0, \omega_1, \omega_2, \dots) \equiv \omega$, where $\omega_0 \geq \omega_1 \geq \omega_2 \geq \dots$ is arranged in a non-increasing order. Similarly, the eigenvalues of ρ'_A are $(\omega'_0, \omega'_1, \omega'_2, \dots) \equiv \omega'$. If $\sum_{j=0}^k \omega_j \leq \sum_{j=0}^k \omega'_j$ for all k , we say that ω is majorized by ω' . [13]. The conversion from $|\psi_{AB}\rangle$ to $|\psi'_{AB}\rangle$ needs a catalyst if ω is not majorized by ω' . Otherwise, the catalyst is not necessary.

In this paper, we elaborate on the idea that the detection of the entanglement structure encoded in the quantum phases of matter is possible through the study of its local convertibility properties[14, 15]. We study the Differential Local Convertibility (DLC), which is defined as the convertibility between two ground states $|\psi(g)\rangle$ and $|\psi(g + \epsilon)\rangle$, corresponding to two Hamiltonians described by parameters g and $g + \epsilon$ (where ϵ is an infinitesimal value). Such an approach has been applied to quantum phases with meaningful order parameter [14–16] and topological phases of two dimensional[17, 18] and one dimensional (1d) [19] spin models (the latter are examples of class of spin liquids known as Symmetry-Protected Topological phases [20–22]; see Ref. 23–25 for an example raised in quantum technology recently). From these studies, we found that while disordered and symmetry broken phases are generically convertible, the topological phases are not and they violate the DLC property. Such property ultimately depends on the interplay between the spin-spin correlation length and the size of the partition: When the subsystem size is smaller than the correlation length between the edge states (found at the interface between A and B) then the edge states can dominate this convertibility. In this case, the ground state are not DLC. In the opposite limit the states are DLC. Such picture is also confirmed by the recent study on the Kitaev chain with a quenched chemical potential [26]. Interestingly, in the cases of large partitions, it was found [27] that DLC can detect specific symmetries of the system.

Most of the current studies analyzed the quantum phase transition across two quantum phases. In this paper, we consider a more complex phase diagram with multiple quantum phases. Specifically, we sweep through two consecutive quantum phase transitions, delineating three quantum phases, one of which being an Symmetry Protected Topological Order (SPTO) phase. We believe that this is an interesting case because the occurrence of quantum phase transitions, generally implies specific constraints on the behavior of the Rényi entropies in the

phase diagram of the system. Therefore, we expect that the presence of multiple quantum phase transitions, can lead to an ‘interference’ effect, in particular, the slopes of the Rényi entropies and ultimately the DLC of the quantum phases. To this end, we study the spin-1/2 XXZ chain with bond alternation whose phase diagram is provided in Fig. 1(b). The techniques we employ are DMRG with periodic boundary conditions [28] and the correlation function matrix [29, 30]. We study the DLC through an analysis of the Rényi entropies. We study the majorization condition as well. The question we wish to study is whether we can characterize the different phases of the phase diagram in terms of the need for a catalyst. Incidentally, we note that just like the model studied in [27], our model can display an $SU(2)$ symmetry non-critical point within the SPTO phase. We analyze the DLC at that point to leverage the analysis carried out in [27].

The paper is organized as follows. In Sec. II, the model of spin-1/2 XXZ chain with bond alternation is introduced and the calculation method is discussed. In Sec. III, the results on DLC are presented. For the topological phase, the mechanism of edge states recombination is used to interpret the inconvertibility. For the Néel phase, the three-phase mechanism is used to interpret inconvertibility. Finally, the conclusion is given in Sec. IV.

II. MODEL AND METHOD

The Hamiltonians of the 1d spin-1/2 alternating XXZ model reads

$$H = \sum_{n=1}^N [1 + (-1)^n \delta] (\sigma_n^x \sigma_{n+1}^x + \sigma_n^y \sigma_{n+1}^y + \Delta \sigma_n^z \sigma_{n+1}^z). \quad (2)$$

Here, $\vec{\sigma}_n$ are the Pauli matrices on the n th site of the chain with N spins. Periodic boundary conditions, $\vec{\sigma}_{N+1} \rightarrow \vec{\sigma}_1$, are applied. Δ is the strength of the Ising-type anisotropy which originates from the spin-orbit interaction in magnetic materials. δ is the bond alternation describing the dimerization by the spin-Peierls instability. The ground-state phase diagram is displayed in Fig. 1(b). We remark that we have drawn it using the finite-size scaling of Rényi entropies and the second derivative of ground state energy. Other methods such as the von Neumann entropy and the ground-state fidelity have been used to obtain a schematic phase diagram. [31] The Hamiltonian can be experimentally realized in ion traps and optical lattices, where the bond alternation is achieved by fine tuning the intensity of the Raman laser beams. [32–34]

The isotropic limit of the model ($\Delta = 1$) has been studied intensively. [35–39] By choosing the unit cell (site $2n-1$ and $2n$), as shown in Fig. 1(a), the ground state for $\delta > 1$ (ferro-antiferromagnetic alternation) is numerically shown [36, 38] to approach the spin-1 Haldane system with a finite value of the non-local string order parameter. The nearest two spins in two different unit cells

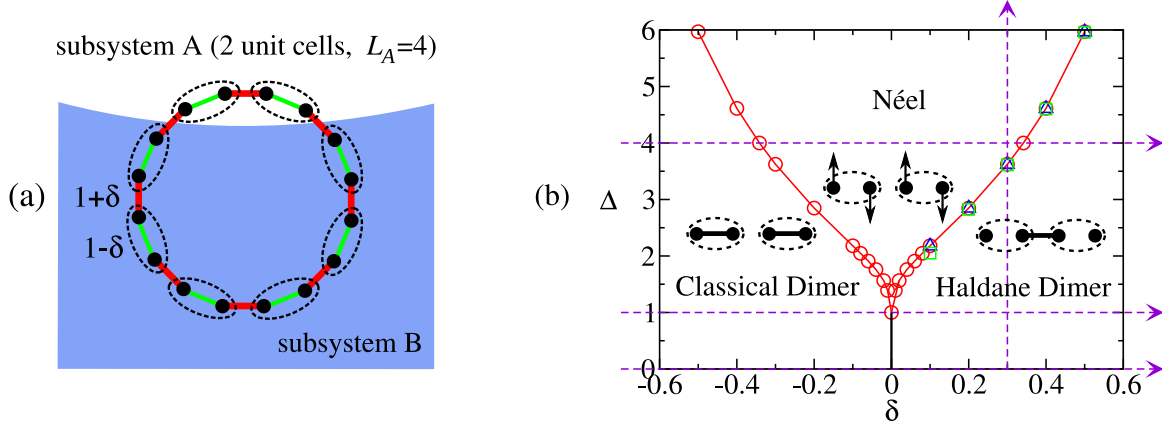


FIG. 1. (color online) (a) The bond alternating spin-1/2 XXZ model with length N . The dashed ellipses define $N/2$ unit cells of the system. The coupling strength of spins in the unit cell is $1 - \delta$ (green lines), and between nearest units is $1 + \delta$ (red lines). The subsystem A contains complete unit cells. (b) The quantum phase diagram of the model is determined by using the finite-size scaling of Rényi entropies S_2 (\triangle), S_∞ (\square) and the second derivative of ground state energy (\circ). The four dashed lines denote the routes that will be swept along in Sec. III.

tend to form a dimer (singlet) or the so-called valence bond, and the unit cells approaches to a spin-1 chain, as described by Affleck, Kennedy, Lieb, and Tasaki. [22] The ground state does not break the translational symmetry by translating a unit cell. On the other hand, a small dimerization $\delta > 0$ breaks the translational symmetry (translating a lattice site) and opens a spin gap from the gapless Luttinger liquid state. The ground state becomes static dimers. Since it has been shown that there is no quantum phase transition between the dimer region ($0 < \delta \leq 1$) and the Haldane region ($\delta > 1$), [36] we refer to the phase as the Haldane-Dimer (HD) phase. On the other hand, for $\delta < 0$, the unit cells tend to form dimers, and the ground state tends to be product over all unit cells. We therefore refer to the phase as the Classical Dimers (CD). Note that after choosing the unit cell, one can distinguish the HD from CD by studying the parity of the entanglement between subsystem A and B (in order to detect entanglement, the subsystem A should contain complete unit cells, *i.e.* the size of the subsystem A, L_A should be even).

In the absence of bond alternation $\delta = 0$, the model can be solved using the Bethe ansatz, and the ground-state phase diagram exhibits ferromagnetic ($\Delta \leq -1$), Luttinger liquid ($-1 < \Delta \leq 1$), and the Néel ($\Delta > 1$) phases. [40] The phase boundaries for $\delta > 0$ and $\delta < 0$ are symmetric by translation of elementary lattice spacing. In the limit of $\Delta \rightarrow \infty$, the ground state is expected to manifest the antiferromagnetic Néel order ($\uparrow\downarrow\uparrow\downarrow$) for $\delta < 1$ and double Néel order ($\uparrow\uparrow\downarrow\downarrow$) for $\delta > 1$, separated by the decoupled line $\delta = 1$. Both Néel states are nearly trivial product states.

In this paper, we focus on studying the Differential Local Convertibility (DLC), and study the edge states in the HD phase and the transitions from HD to the Néel phase, from CD to HD phase, as well as from CD to Néel phase and then to HD phase. Therefore, only the region

$\Delta > 0$ and $-1 < \delta < 1$ is present. See Fig. 1(b) for the four routes (the dashed lines) that will be swept along in Sec. III.

The DLC relies on the calculation of the correlation matrix of (2). By the Jordan-Wigner transformation, Eq. (2) can be mapped into spinless fermion chain. When $\Delta = 0$, the model is exactly solvable [29, 30, 41, 42] for both finite N and in the thermodynamic limit $N \rightarrow \infty$, see Appendix A for details. When $\Delta \neq 0$, we solve it numerically. We use the Density Matrix Renormalization Group (DMRG) method [43] with the recently developed parity scheme. [28] Unlike the quantum Monte Carlo methods which may only simulate the Rényi entropy S_α with integer $\alpha \geq 2$, [44–46] the DMRG allows to compute S_α with a wide range of α . As we will present in this work, α is taken from 10^{-2} to 10^3 . The parity scheme of DMRG [28] enables us to label the eigenstates of ρ_A by the quantum numbers S_A^z and p_A , where $S_A^z = \frac{1}{2} \sum_{n \in A} \sigma_n^z$ is the z -component of total spins and p_A is the parity (inversion) of the subsystem A. Thus the eigenvalues and eigenstates of ρ_A can be identified by (S_A^z, p_A) , which helps to better characterize the topological system.

III. DIFFERENTIAL LOCAL CONVERTIBILITY

In this section, we shall present the results of DLC within each of the phase diagram Fig. 1.

In the first instance, we study the response of the ES to the sweep.

DLC is concerned with the convertibility between the ground state $|\psi(g)\rangle$ and $|\psi(g+\epsilon)\rangle$ of Eq. (2). The DLC can be related to the derivative of the Rényi entropies: $\frac{\partial S_\alpha}{\partial g}$. If the latter is non-negative, then $|\psi(g)\rangle$ can be converted to $|\psi(g+\epsilon)\rangle$, while the conversion changes direction otherwise. DLC breaks down if $\frac{\partial S_\alpha}{\partial g} \leq 0$ changes

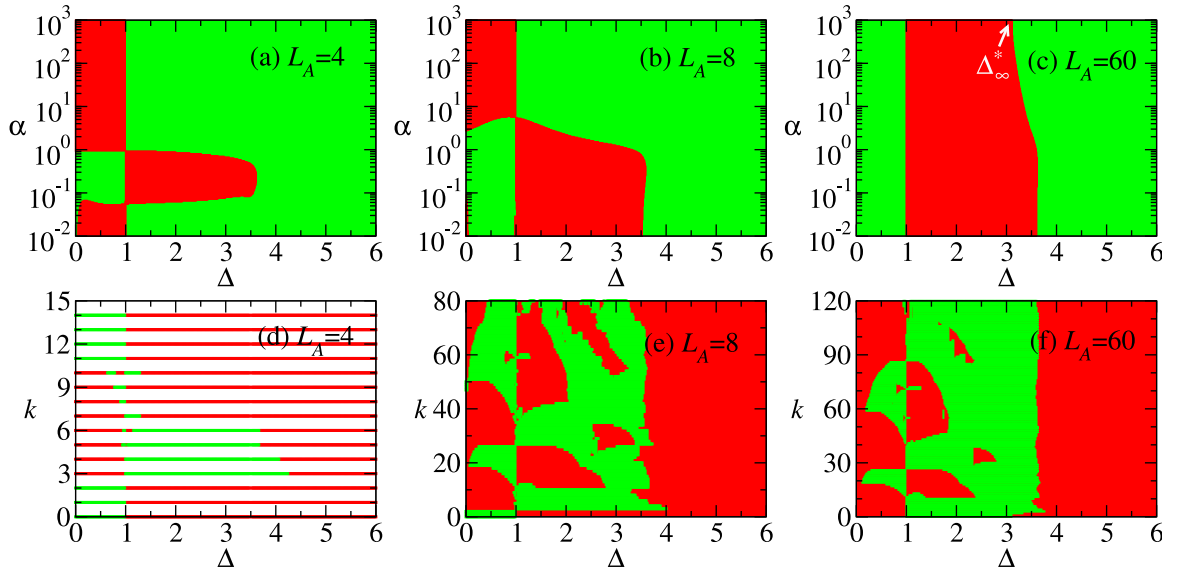


FIG. 2. (color online) (a), (b), (c) The sign of $\frac{\partial S_\alpha}{\partial \Delta}$ is plotted against Δ , where S_α is the Rényi entropy of the reduced state of subsystem A with size $L_A = 4, 8, 60$ as marked in the graphs. (d), (e), (f) The corresponding plots of majorization $M(k)$. The red color denotes that $\frac{\partial S_\alpha}{\partial \Delta} > 0$ ($M(k) > 0$) and the green color indicates that $\frac{\partial S_\alpha}{\partial \Delta} < 0$ ($M(k) < 0$). The parameters are $N = 120$, $\delta = 0.3$, $\epsilon = 5 \times 10^{-3}$. In the DMRG calculation, $m = 600$ states are kept, with the truncation error below 10^{-12} .

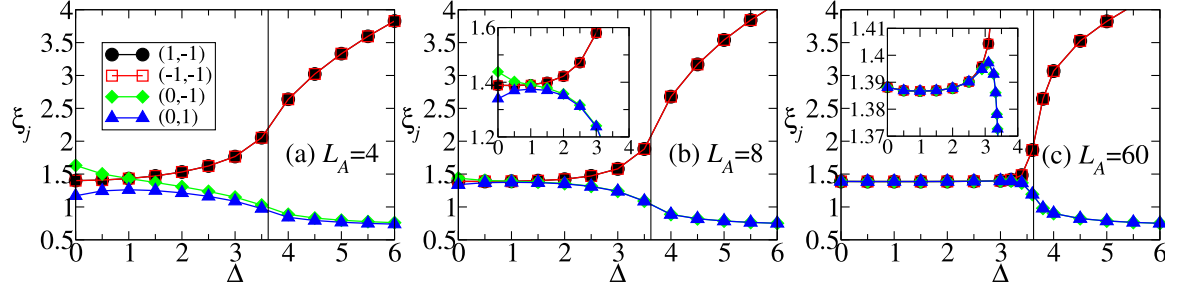


FIG. 3. (color online) (a), (b), (c) The lowest four eigenvalues of the entanglement Hamiltonian H_E , $e^{-H_E} = \rho_A$, corresponding to Fig. 2(a), (b), (c). Each line is labelled with the quantum numbers (S_A^z, p_A) , where $S_A^z = 0, \pm 1$ and $p_A = \pm 1$. See also the last paragraph of Sec. II. The insets of (b) and (c) are the zoom-in of (b) and (c). The vertical line denotes the critical point $\Delta_c \approx 3.623$ obtained by the energy derivatives.

sign with α .

We also considered the majorization between $|\psi(g)\rangle$ and $|\psi(g+\epsilon)\rangle$. In this way, we can study whether the catalyst is needed in the convertibility. The majorization between $|\psi(g)\rangle$ and $|\psi(g+\epsilon)\rangle$ is defined as

$$M(k) = \frac{\partial}{\partial g} \sum_{j=0}^k \omega_j, \quad (3)$$

where ω_j 's are the eigenvalues of the reduced state of the subsystem. The local conversion between $|\psi(g)\rangle$ and $|\psi(g+\epsilon)\rangle$ without the aid of a catalyst is possible if the sign of $M(k)$ is uniform up to 0 (see Sec. I).

A. Sweeps along Δ

Here, we compute the DLC along the vertical sweep in Fig. 1.

Fig. 2(a), (b), (c) show the sign of $\frac{\partial S_\alpha}{\partial \Delta}$ for $0 \leq \Delta \leq 6$, $10^{-2} \leq \alpha \leq 10^3$, $\delta = 0.3$ and $N = 120$. The subsystem size $L_A = 4, 8, 60$. Fig. 2(d), (e), (f) show the corresponding plots of majorization. We observe that, for a generic partition, the ground state in the HD cannot be converted. Nevertheless, we observe that the convertibility tends to be restored by increasing the partitions size. This phenomenon arises since the resources encoded in larger systems increase; therefore the convertibility is enhanced. This argument applies to one of the two subsystems whose size does not exceed $N/2$, as the effect of LOCC is more restricted by this subsystem rather than the other one (similar to the Schmidt decomposition of bipartite states). In view of this property, we fix the total

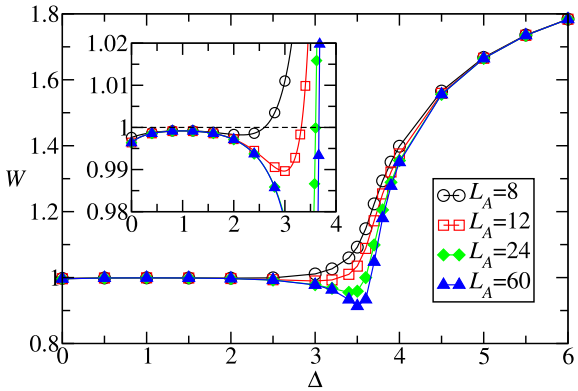


FIG. 4. (color online) The quantity $W = 4 \sum_j \omega_j^2$ is plotted against Δ for $L_A = 8, 12, 24, 60$. The inset is the zoom-in plot.

size of the Hamiltonian and vary the size of subsystem A.

It can be seen in Fig. 2(a), (b), (c) that for $L_A = 4, 8$, DLC breaks down when $0 \leq \Delta \lesssim 3.6$, while it is positive when $\Delta \gtrsim 3.6$. We notice that the critical point $\Delta_c \approx 3.623$ separates the topological phase ($0 \leq \Delta < \Delta_c$) from the non-topological Néel phase ($\Delta > \Delta_c$). It is also found that the inconvertible region in Fig. 2(c) shrinks when $L_A = N/2$ increases. We will examine it numerically in Appendix B, where it is shown that the inconvertible region disappears in the thermodynamic limit.

Combining Figs. 2(c) with 2(f), it can be seen that the *local conversion needs a catalyst in most part of the topological phase*, except around $\Delta = 0$ and $\Delta = 3$. In comparison, the catalyst is not necessary in the Néel phase. The local conversion changes direction at the SU(2) symmetry point $\Delta = 1$ where the majorization shows a mirror-like symmetry. Moreover, it is conceivable that in the thermodynamic limit the conversion direction changes at the critical point $\Delta_c \approx 3.623$. This is because the local conversion cannot increase the entanglement which diverges at the critical point (quantified by the von Neumann entropy, see Fig. 2(c) with $\alpha = 1$).

In the following, we shall argue that the behavior of DLC can be understood in terms of edge states formation. Fig. 3(a), (b), (c) show the lowest four eigenvalues of the entanglement Hamiltonian H_E , $e^{-H_E} = \rho_A$, for the three cases in Fig. 2. Let us consider $L_A = 60$ first. It can be seen that the four eigenvalues of the reduced density matrix are almost degenerate in the HD phase. See also the zoom-in plot in Fig. 3(c). Moreover, it is numerically found that the whole ES is at least four-fold degenerate. This suggests that the reduced state of subsystem A is approximately

$$\rho_A \approx \begin{bmatrix} \frac{1}{2} & 0 \\ 0 & \frac{1}{2} \end{bmatrix} \otimes \rho_0 \otimes \begin{bmatrix} \frac{1}{2} & 0 \\ 0 & \frac{1}{2} \end{bmatrix}, \quad (4)$$

where ρ_0 is a $2^{L_A-2} \times 2^{L_A-2}$ matrix whose eigenvalues are equal to four times the eigenvalues of ρ_A . The two identical 2×2 matrices in Eq. (4) can be identified as

the two edge states which induce the four-fold degeneracy of ES. This identification, manifesting the edge-ES correspondence. [47–49], is supported by the two limiting cases below. (i) When $\delta = 1$, the model is simplified as the sum of disconnected two-body XXZ Hamiltonians. The ground state is a tensor product of spin singlet states. If the subsystem A is chosen in such a way that both of its boundaries cut the singlet states, its reduced state is exactly the form in Eq. (4). The state ρ_0 is a pure state composed of singlet states of the bulk, while the other two identical matrices originate from the partial trace of the singlet states at the boundaries. (ii) When $\Delta = 0$, Eq. (2) is equivalent to the Hamiltonian of non-interacting fermions, through the Jordan-Wigner transformation. See Appendix A for details. In this case, the reduced state of the subsystem can be expressed as $\rho_A = e^{-\sum_k \varepsilon_k \tilde{c}_k^\dagger \tilde{c}_k}$ up to normalization. Here $\tilde{c}_k^\dagger, \tilde{c}_k$ are the creation, annihilation operators of the eigenmodes confined in the subsystem A with energy ε_k . When the subsystem is sufficiently long and its two boundaries cut the stronger bonds (with coupling strength $1 + \delta, \delta > 0$), there will be two eigenmodes which are localized about the boundaries with negligible energy, say, $\varepsilon_1 \approx \varepsilon_2 \approx 0$. As a result, the reduced state ρ_A can be written in the form of Eq. (4). For general cases ($\Delta \neq 0$ and $\delta \neq 1$), the ground state and the reduced state accordingly are complex many-body states. The four-fold ES degeneracy can be used to detect the edge states. [50]

In Fig. 4, the quantity $W = 4 \sum_j \omega_j^2$ is plotted vs Δ , where $N = 120$, $L_A = 8, 12, 24, 60$ and ω_j 's are the eigenvalues of the reduced state of the subsystem A. The quantity W with a large subsystem size basically shows the purity of the bulk ρ_0 : $\text{tr}(\rho_0^2) \approx 4\text{tr}(\rho_A^2) = 4 \sum_j \omega_j^2$. It reflects the correlation between the bulk sites and the two edges, as interpreted below. Fig. 4 shows that the purity of the bulk state increases with Δ to reach a maximum at $\Delta = 1$, and then it starts to decrease. This behavior indicates that the bulk sites become less correlated with the two edges when Δ increases to approach 1, while they do the opposite when $\Delta > 1$. This point can be understood by considering the special case $\delta = 1$ where the bulk state is a pure state composed of singlet states so that the bulk sites are completely uncorrelated with the edges. Therefore, the lowest four eigenvalues of H_E have a local minimum at $\Delta = 1$, where they are closest to $-\ln 0.25 \approx 1.386$. See the inset of Fig. 3(c). The bifurcation occurs when $\Delta \gtrsim 3.1$, showing that the four-fold ES degeneracy is partially lifted. As a consequence, Eq. (4) is no longer applicable. It's conceivable that the edge states start recombining, resulting in the splitting of the lowest four eigenvalues of H_E . In particular, $\xi_0 \equiv -\ln \omega_0$ will decrease with Δ .

The above analysis is consistent with DLC in Fig. 2(c). Since $\lim_{\alpha \rightarrow \infty} S_\alpha(\rho_A) = -\ln \omega_0$, the sign of $\frac{\partial S_\alpha}{\partial \Delta}$ for large α in Fig. 2 can be derived from Fig. 3(f). In addition, when $\alpha \rightarrow 1$, the Rényi entropy reduces to the von Neumann entropy which has been shown to diverge at critical points. [51–53] This result was verified in the spin-1/2

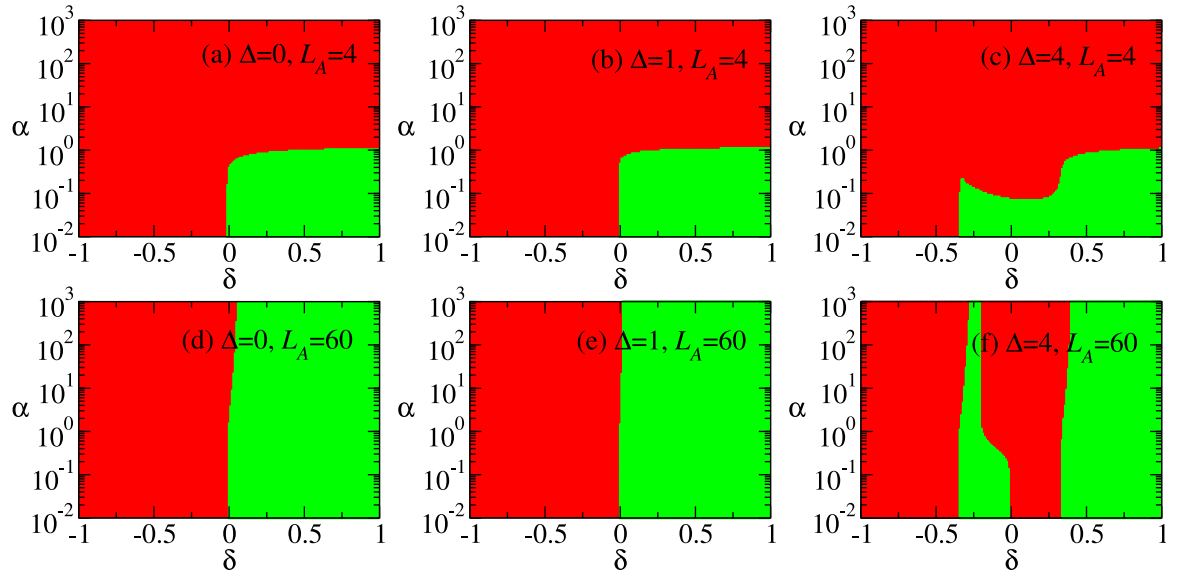


FIG. 5. (color online) The sign of $\frac{\partial S_\alpha}{\partial \Delta}$ are plotted against δ , where S_α is the Rényi entropy of the reduced state of subsystem A. (a), (b), (c) The subsystem size $L_A = 4$, $\Delta = 0, 1, 4$. (d), (e), (f) $L_A = 60$, $\Delta = 0, 1, 4$. The total size is $N = 120$ ($N \rightarrow \infty$ for $\Delta = 0$). In the DMRG calculation, $m = 300$ states are kept for $\Delta = 4$, with the truncation error below 10^{-11} near the critical points, and below 10^{-14} away from the critical points.

XXZ chain with bond alternation. [31]

Next, we consider $L_A = 4, 8$. Comparing Fig. 2(a), (b) with (c), we find that the inconveritible region in Fig. 2(c) increases when the subsystem size decreases. Namely, the ground state changes from convertible to non-convertible at Δ that becomes smaller when L_A decreases. This indicates that the edge states start recombining at smaller Δ when L_A decreases. Note that $\Delta = 1$ no longer separates the positive and negative DLC regions: all the regions in HD phase are locally inconveritible due to the recombination of edge states for small L_A .

In the final part of the present subsection, we shall give a physical interpretation for Fig. 3(a), (b). Roughly speaking, the term $\sum_n \Delta \sigma_n^z \sigma_{n+1}^z$ tends to anti-parallel the z components of neighboring spins, which has an effect that the z components of spins of the two edges of subsystem A are also anti-parallel. Thus, the probability ω_j of the eigenstates with quantum number $(S_A^z, p_A) = (0, -1)$ of ρ_A increases with Δ . These eigenstates are the anti-parallel component of the triplet states with $p_A = -1$. Based on this picture, the change of ES ($\xi_j = -\ln \omega_j$) when Δ is varied, as shown in Fig. 3(a), (b), can be understood. Both the Schmidt states with quantum number $(0, -1)$ and those with $(0, 1)$ have anti-parallel z components of spins for the two edges. The reason why the term $\sum_n \Delta \sigma_n^z \sigma_{n+1}^z$ prefers the former to the latter when $0 \leq \Delta \leq 1$ is related to the ES level crossing at the SU(2) symmetry point $\Delta = 1$. We notice that due to the level crossing, the sign of the derivative of Rényi entropy flips at $\Delta = 1$ for all α . This means that the ES of the singlet state with quantum number $(0, 1)$ has an extreme point at $\Delta = 1$ and around it a mirror-like symmetry is present. [27]

The reduced state of the special case $\Delta = 0$ is shown in Eq. (A7). It can be seen in Fig. 3(a), (b) that the ES splitting becomes smaller when Δ increases from 0 to 1, and then it becomes larger when Δ increases further. These results indicate that there is a minimum recombination of the edge states at $\Delta = 1$. Beyond the critical point, the edge states disappear and the system goes to the Néel phase. In this phase the ground state is convertible.

B. Sweeps along δ

Fig. 5 shows the sign of $\frac{\partial S_\alpha}{\partial \Delta}$ for $-1 \leq \delta \leq 1$, $10^{-2} \leq \alpha \leq 10^3$, $\Delta = 0, 1, 4$ and $L_A = 4, 60$. The case $\Delta = 0$ is calculated by using the correlation matrix formalism in Appendix A with $N \rightarrow \infty$. For $\Delta = 1, 4$, DMRG is used and $N = 120$. The topological regime is $0 < \delta \leq 1$ for $\Delta = 0, 1$, and $0.34 \lesssim \delta \leq 1$ for $\Delta = 4$.

Fig. 5 shows that DLC cannot be achieved within the topological phase, at small sizes L_A . These results can be interpreted by the recombination of edge states (see the previous subsection). The inconveritible region in the topological phase shrinks when L_A increases, and it will disappear in the thermodynamic limit (this will be discussed in Appendix B). This phenomenon was also discussed in the previous subsection. In contrast with the sweep along Δ , however, the local conversion in *part of the convertible topological phase does not need the catalyst*. See Fig. 6 for the majorization. This indicates that in the large L_A limit, the phases cannot be told apart neither by looking at the necessity of the catalyst.

In contrast with the previous sweep, the DLC can be

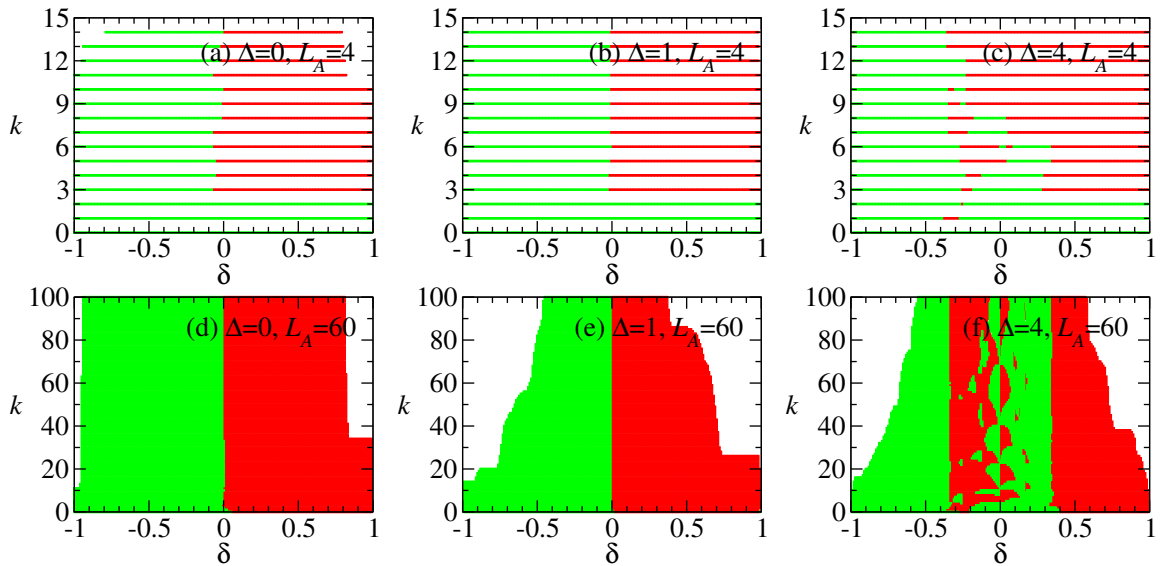


FIG. 6. (color online) (a), (b), (c), (d), (e), (f) are the six plots of majorization corresponding to the six plots in Fig. 5 respectively. The numerical error in the calculation of the eigenvalues of the reduced density matrix is below 10^{-13} . The points with $|\sum_{j=0}^k \omega_j(\delta + \epsilon) - \omega_j(\delta)| < 10^{-13}$ are not shown, where $\epsilon = 5 \times 10^{-3}$. These points are mainly located at $|\delta|$ close to 1.

violated within the Néel phase, Fig. 5(c), and Fig. 5(f). As detailed below, such a phenomenon arises because of the two consecutive continuous quantum phase transitions bounding the Néel phase. The sweep along δ goes through three phases: CD, Néel and HD. Since the Rényi entropies diverge at the two critical points $\delta \approx \pm 0.34$ for infinite L_A , there must be two maxima respectively around the two points for large L_A . Apparently, a minimum between the two maxima is present for every α , as can be seen in Fig. 5(f). The value of δ corresponding to this minimum in general varies with α (unless some additional symmetry is present in the subsystem A, like the SU(2) at $\Delta = 1$ in Fig. 2(c), but it does not seem to exist here). As a result, that specific Néel phase may result unconvertible. For small L_A , the value of α corresponding to a negative derivative of the Rényi entropy is small: $10^{-2} \lesssim \alpha \lesssim 10^{-1}$. See Fig. 5(c). This is understood as the residual influence of the above three-phase mechanism on the Rényi entropies. Fig. 7(a) shows the Rényi entropy for various values of small α . It can be seen that in the Néel phase, the Rényi entropy decreases very slowly for $10^{-2} \lesssim \alpha < 10^{-1}$. In contrast, it decreases rapidly in the HD phase.

The behavior of the small- α Rényi entropies can be understood by inspecting the entanglement spectrum, as shown in Fig. 7(b). It can be seen that in the Néel phase, the eigenvalues of the entanglement Hamiltonian, ξ_j 's, are smaller than 18. The corresponding eigenvalues of ρ_A are larger than $e^{-18} \approx 1.5 \times 10^{-8}$. Thus, the rank of ρ_A is 16 which is unchanged with δ . Also, the large ξ_j 's increase slowly with δ , as compared with their change in the HD phase. Some of them even decreases. Since the small- α Rényi entropies are susceptible to the large ξ_j 's, their slow decrease with δ is understood. In the

HD phase, the large ξ_j 's increases rapidly with δ , resulting in a rapid decrease of the effective rank of ρ_A . The rapid decrease is a consequence of the formation of the edge states when δ approaches 1: the small eigenvalues of ρ_A disappears and only the four largest eigenvalues dominates. Therefore, the small- α Rényi entropies, representing the effective rank of ρ_A , also decrease rapidly with δ .

IV. CONCLUSION

In this paper, we have investigated the entanglement convertibility in the one-dimensional spin-1/2 XXZ model with bond alternation. The phase diagram is parametrized by the Ising-type anisotropy Δ and the bond alternation δ (see Fig. 1(b)). We sweep both in Δ (fixed δ) and in δ (fixed Δ). The method we exploit for calculating the Rényi entropies is the DMRG with parity quantum numbers [28] and the correlation function matrix formalism [29, 30], applied to systems with periodic boundary condition. Such calculations are carried out by a bipartition of the system A|B with blocks of length L_A , L_B , and tracing out B. The finite-size scaling of the maximum of Rényi entropies S_α with $\alpha \rightarrow \infty$ and $\alpha = 2$ are used to locate the critical point. It is compared with the finite-size scaling of second derivatives of ground state energy density and they agree well. The precise ground-state phase diagram is determined.

Our results confirm that response of the entanglement spectrum is markedly different in topological and non-topological phases: The effective rank of the reduced density matrix changes much faster in the topological phase than in the Néel phase. As detailed below, such a phe-

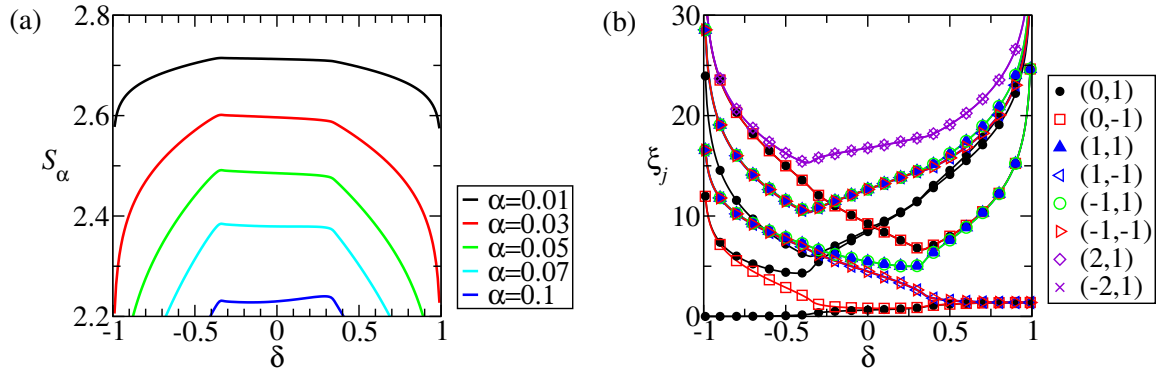


FIG. 7. $\Delta = 4$ and $L_A = 4$. (a) The small- α Rényi entropies ($\alpha = 0.01, 0.03, 0.05, 0.07, 0.1$) and (b) the entanglement spectrum, $\xi_j = -\ln \omega_j$, corresponding to Fig. 5(c). The number pairs in the legend denote the values of the quantum numbers (S_A^z, p_A).

nomenon is responsible for the violation of DLC within the topological Haldane dimer phase at small L_A .

Differential Local Convertibility. Our results confirm that the DLC depends on the ratio between the spin-spin correlation length and the size of the partition. In agreement with the Ref. 27, our results obtained in the case of large subsystems indicate that the direction of local conversion is reversed at the SU(2) symmetry point. In agreement with the Ref. 19, for a small subsystem size, the state results unconvertible within the SPTO Haldane dimer phase, for both sweeps in Δ and δ . Such a result arises as a recombination of edge states as in Ref. 16. The ground state results DLC within the classical Dimer phase. In contrast with the case analyzed in previous studies, however, the DLC changes within the Néel phase. This phenomenon is a specific effect of the presence of the two continuous quantum phase transitions bounding the Néel phase: Since the Rényi entropies diverge at the two critical points δ_c for infinite L_A , there must be two maxima respectively around the two points for large L_A . Apparently, a minimum between the two maxima is present for every α , as can be seen in Fig. 5(f). The value of δ corresponding to this minimum in general varies with α (unless some additional symmetry is present in the subsystem A, like the SU(2) at $\Delta = 1$ in Fig. 2(c), but it does not seem to exist here). As a result, negative DLC emerges in the Néel phase.

Majorization. We find the conversion fulfills the majorization relation in the non-topological phases. In the sweep along δ in the topological phase, the conversion violates the majorization relation, even in the large L_A limit. This result indicates that the catalyst is strictly necessary in the process. In the sweep along Δ , however, the catalyst seems not needed in the part of the topological phase.

Overall, our study can provide a characterization of the topological order through the response of the entanglement spectrum, on a local scale. This may facilitate the experimental sought of topological order [54]. On the more quantum information side, our results contribute to the questions on whether topological phases universally

encode more computational power than non-topological phases.

ACKNOWLEDGMENTS

L.D and M.C.C. are grateful to MOST in Taiwan for the financial supports via MOST-104-2811-M-005-012 and NSC102-2112-M-005-001-MY3, respectively. Y.C.T. is grateful to Prof. Guang-Yin Chen and Prof. Wen-Min Huang for providing computing facilities. L.C.K. acknowledges support from the National Research Foundation & Ministry of Education, Singapore.

Appendix A: Dimerized chain of non-interacting spinless fermions

When $\Delta = 0$, the Hamiltonian in Eq. (2) can be mapped to the dimerized chain of non-interacting spinless fermions [41] through the Jordan-Wigner transformation, and the entanglement spectrum can be computed using the correlation function matrix (CFM) formalism. [29, 30]

The Jordan-Wigner transformation is

$$c_j = \sigma_j \prod_{k=1}^{j-1} (-\sigma_k^z), \quad (A1)$$

where $\sigma_j = (\sigma_j^x - i\sigma_j^y)/2$. Substituting Eq. (A1) into Eq. (2), we have

$$\begin{aligned} H = & -2 \sum_{n=1}^{N-1} [1 + (-1)^n \delta] (c_n c_{n+1}^\dagger + c_{n+1} c_n^\dagger) \\ & + 2[1 + (-1)^N \delta] (c_N c_1^\dagger + c_1 c_N^\dagger) \prod_{j=1}^N (1 - 2c_j^\dagger c_j). \end{aligned} \quad (A2)$$

Assume N is an even number and $M = N/2$. Since the number operator $\sum_j c_j^\dagger c_j$ commutes with the Hamiltonian, the eigenstates of the Hamiltonian can be solved

in the subspace of conserved number of particles. In particular, it will be shown later that the ground state is non-degenerate and contains M particles (*i.e.* half-filled) when $\delta \neq 0$. In this case, the operator $\prod_{j=1}^N (1 - 2c_j^\dagger c_j)$ in Eq. (A2) is equal to $(-1)^M$. Thus, we have a free fermion chain with periodic boundary conditions (PBC) when M is odd, while the boundary condition is anti-periodic when M is even.

Perform the Fourier transformation

$$c_{2j-1} = \frac{1}{\sqrt{M}} \sum_{k=1}^M a_k e^{i \frac{p_k \pi}{M} j}, \quad (\text{A3})$$

$$c_{2j} = \frac{1}{\sqrt{M}} \sum_{k=1}^M b_k e^{i \frac{p_k \pi}{M} j}, \quad (\text{A4})$$

where p_k depends on M : when M is odd, $p_k = 2k$, otherwise $p_k = 2k + 1$. The choice of p_k is to ensure that the Fourier transformation works for both PBC and anti-PBC fermion chains. The Hamiltonian is transformed into

$$H = \sum_{k=1}^M [a_k^\dagger \ b_k^\dagger] [\mathbf{R}(k) \cdot \boldsymbol{\sigma}] \begin{bmatrix} a_k \\ b_k \end{bmatrix}, \quad (\text{A5})$$

where $\mathbf{R}(k) = (R_x(k), R_y(k), R_z(k))$, $R_x(k) = 2(1 - \delta) + 2(1 + \delta) \cos \frac{p_k \pi}{M}$, $R_y(k) = 2(1 + \delta) \sin \frac{p_k \pi}{M}$, $R_z(k) = 0$, and $\boldsymbol{\sigma} = (\sigma_x, \sigma_y, \sigma_z)$ is the vector of Pauli matrices. The length of $\mathbf{R}(k)$ is $R(k) = 4\sqrt{\cos^2 \frac{p_k \pi}{2M} + \delta^2 \sin^2 \frac{p_k \pi}{2M}}$. The Hamiltonian has two bands with energy $\pm R(k)$. When $\delta \neq 0$, $R(k)$ is nonzero for all k and the two bands are gapped. The ground state corresponds to the occupied negative-energy band (half-filled) and it is non-degenerate. When $\delta = 0$, the Hamiltonian is gapless, since the two bands touch when $M \rightarrow \infty$ ($R(k) \rightarrow 0$ for $p_k/M \rightarrow 1$).

The topological properties of the chain can be characterized by the Berry phase [42] $\gamma \equiv \int_0^{2\pi} dk \langle \phi | i \partial_k | \phi \rangle$, where $|\phi\rangle$ is the eigenvector of $\mathbf{R}(k) \cdot \boldsymbol{\sigma}$ with the eigenvalue $-R(k)$. It can be shown that $\gamma = n_w \pi$ modulo 2π , where $n_w \equiv \frac{1}{2\pi} \int_0^{2\pi} \frac{d\theta}{dk} dk = [1 + \text{sign}(\delta)]/2$. Here θ is the polar angle: $\tan(\theta) = R_y(k)/R_x(k)$. The quantity n_w is the winding number describing the total number of times that $\mathbf{R}(k)$ surrounds the origin of the $(R_x(k), R_y(k))$ parametric space when k changes from 0 to 2π . A nonzero n_w (*i.e.* $\delta > 0$) defines the topological phase, where the chain with open-boundary conditions supports two edge modes. For PBC, the reduced state of subsystem has two edge modes when two stronger bonds are cut off. This can be derived by the CFM below.

The CFM is defined as $C_{m,n} = \langle \phi_0 | \mathbf{c}_m \mathbf{c}_n^\dagger | \phi_0 \rangle$, where $|\phi_0\rangle$ is the ground state and $\mathbf{c}_m = [c_{2m-1} \ c_{2m}]^T$. It can be verified that $C_{m,n} = \frac{1}{M} \sum_k e^{i \frac{p_k \pi}{M} (m-n)} G(k)$, where $G(k)$ is the CFM in momentum space: [30]

$$G(k) = \frac{1}{2} [I_{2 \times 2} + \hat{\mathbf{R}}(k) \cdot \boldsymbol{\sigma}], \quad (\text{A6})$$

where $\hat{\mathbf{R}}(k) = \mathbf{R}(k)/R(k)$ is a unit vector. The reduced state of subsystem A is $\rho_A = \frac{1}{Z} e^{-\sum_l \varepsilon_l \tilde{c}_l^\dagger \tilde{c}_l}$,

where $Z = \text{tr}(e^{-\sum_l \varepsilon_l \tilde{c}_l^\dagger \tilde{c}_l})$ is the normalization constant, $\varepsilon_l = \ln \frac{q_l}{1-q_l}$, $\tilde{c}_l = \sum U_{lm} c_m$, and U is the unitary matrix that diagonalizes the CFM with eigenvalues q_l (*i.e.* $U[C_{m,n}]U^\dagger$ is a diagonal matrix). The reduced state ρ_A can be written compactly as [55] $\rho_A = \det(I - C) e^{\mathbf{c}^\dagger \ln[C(I - C)^{-1}] \mathbf{c}}$, where I is the $L_A \times L_A$ identity matrix and $C \equiv [C_{m,n}]$.

When the subsystem is defined by cutting off two stronger bonds, there will be two zero-energy edge modes, say $q_1 \approx q_2 \approx \frac{1}{2}$. We have

$$\begin{aligned} \rho_A &= \rho_0 \otimes \frac{1}{Z_1} e^{-\varepsilon_1 (\tilde{c}_1^\dagger \tilde{c}_1 - \tilde{c}_2^\dagger \tilde{c}_2)}, \\ &= \begin{bmatrix} \frac{1}{2} - \lambda & 0 \\ 0 & \frac{1}{2} + \lambda \end{bmatrix} \otimes \rho_0 \otimes \begin{bmatrix} \frac{1}{2} + \lambda & 0 \\ 0 & \frac{1}{2} - \lambda \end{bmatrix}, \end{aligned} \quad (\text{A7})$$

where ρ_0 is the reduced state of all the eigen-modes excluding the edge modes, $Z_1 = \text{tr}(e^{-\varepsilon_1 (\tilde{c}_1^\dagger \tilde{c}_1 - \tilde{c}_2^\dagger \tilde{c}_2)})$, ε_1 is positive and equals $\ln \frac{q_1}{1-q_1} \approx 0$, $\lambda = q_1 - \frac{1}{2}$, $\tilde{c}_1^\dagger = \frac{1}{\sqrt{2}} (\tilde{c}_L^\dagger - \tilde{c}_R^\dagger)$, $\tilde{c}_2^\dagger = \frac{1}{\sqrt{2}} (\tilde{c}_L^\dagger + \tilde{c}_R^\dagger)$. Here, $\tilde{c}_L^\dagger, \tilde{c}_R^\dagger$ are the creation operators of the left and right edge modes. The wave function for the edge modes can be derived from the eigenvectors of ρ_A (corresponding to the eigenvalues $q_{1,2}$). The form of $\tilde{c}_{1,2}^\dagger$ is consistent with the requirement that ρ_A commutes with the inversion symmetry operator within subsystem A. Note that Eq. (A7) is a special case of Eq. (4). Also, the two degenerate entanglement spectra at $\Delta = 0$ in Fig. 3(a) can be understood by inspecting the matrix elements of the two edge states in Eq. (A7).

The Rényi entropy of ρ_A when $\Delta = 0$ is simplified as

$$S_\alpha(\rho_A) = \frac{1}{1 - \alpha} \sum_{j=1}^{L_A} \ln[q_j^\alpha + (1 - q_j)^\alpha]. \quad (\text{A8})$$

Appendix B: Phase diagram

In this section, with the finite-size scaling, we study the topological HD phase boundaries. We have shown in the previous section that the topological states are not convertible for a small subsystem $L_A = 4$. However, since the non-topological phase there may also present negative convertibility, one can not in general detect the topological transitions by examining the boundary of convertibility. We therefore look for other quantities in the case of half-half bipartition, $L_A = N/2$, and performing extrapolation to the thermodynamic limit $N \rightarrow \infty$. Recent studies [56] have shown the non-universality of entanglement spectrum and Rényi entropies S_α in the sense that they may exhibit excessive singular changes within the same physical phase. However, S_α can still be used to locate the critical point, since S_α for all α are also singular [57] at the critical point. We concentrate on two special cases of S_α : $\alpha \rightarrow \infty$ and $\alpha = 2$, as they are closely related to DLC. Other values of α can also be considered, which are omitted here.

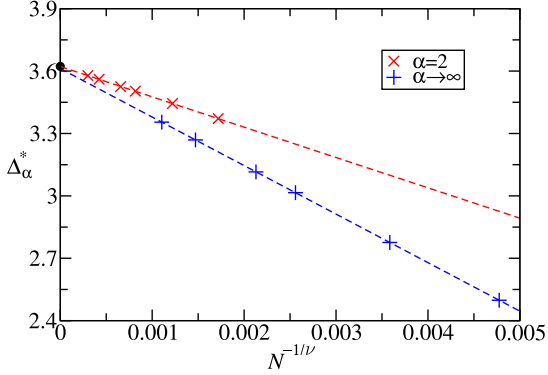


FIG. 8. (color online) Extrapolation of critical points from the Rényi entropies with $\alpha = 2$ and $\alpha \rightarrow \infty$ for the sweeps along Δ while fixing $\delta = 0.3$. The critical point $\Delta_c \approx 3.622$ and 3.612 for $\alpha = 2$ and $\alpha \rightarrow \infty$, with the exponents $\nu \approx 0.653$ and 0.778 , respectively. The black point denotes the critical value of $\Delta_c \approx 3.623$ obtained from the 2nd derivatives of ground state energy.

The sign-changed point Δ_c^* of DLC for infinite α , as pointed out in the Fig. 2(c). This point indicates the beginning of the recombination of edge states. We refer to this point as the pseudo-critical point for a finite N . When $N \rightarrow \infty$, it converges to the infinite system's critical point. We numerically determine the pseudo-critical point Δ_c^* such that $\partial_\Delta S_\infty = \partial_\Delta \xi_0 = 0$, where ξ_0 is the lowest eigenvalue of the entanglement Hamiltonian. When the system size N increases, the shift of this point represents the shrink of the region of negative convertibility. As shown in Fig. 8, Δ_c^* approaches the critical point $\Delta_c \approx 3.612$ in the thermodynamics limit $N \rightarrow \infty$. In fact, the Rényi entropies exhibit logarithmic divergence: $S_\alpha \propto \ln L_A$ in an infinite gapless one-dimensional model. [57] Thus, the extreme point of Rényi entropies must converge to the same critical point when $N \rightarrow \infty$. Now we have more confidence to say that, for fixed δ and varying the anisotropy parameter Δ with half-half bipartition, both the HD phase and Néel phase have positive convertibilities in the thermodynamic limit.

We now consider the Rényi entropy with $\alpha = 2$. There are three advantages. (i) It reflects the purity of ρ_A as $S_2 = -\ln \text{tr}(\rho_A^2)$. It is also related to the quantity W in Fig. 4 and thus the purity of the bulk state ρ_0 when Eq. (4) is valid: $S_2 = -\ln \frac{W}{4} \approx -\ln \frac{\text{tr}(\rho_0^2)}{4}$. (ii) S_2 can be measured directly in experiments without reconstructing the eigenvalues of ρ_A . [54, 58, 59] (iii) In the quantum Monte Carlo methods, for $\alpha = 1$, the von Neumann entropy S_v is difficult to simulate. Rényi entropies with integer $\alpha \geq 2$, especially S_2 is easier to be simulated. [44–46] We numerically determine the pseudo-critical point Δ_2^* by locating the maximum of S_2 , which is also the minimum of W in Fig. 4. As shown in Fig. 8, for $\delta = 0.3$ the critical point $\Delta_c \approx 3.622$ is obtained precisely.

However, when very small value of $\delta \approx 0^+$ is fixed, the HD phase are close to the critical Luttinger liquid for the

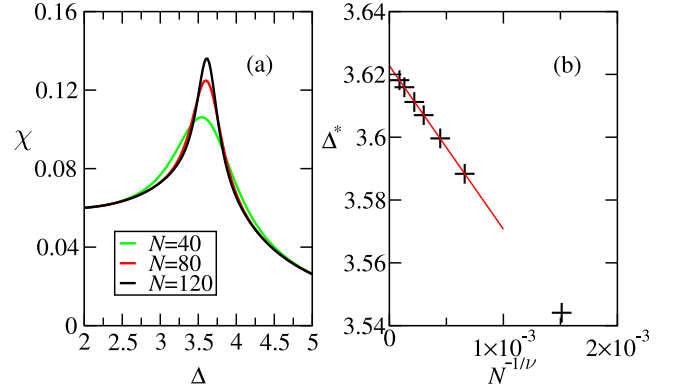


FIG. 9. (color online) (a) The 2nd derivatives of ground state energy density $\chi = -\partial^2 e_0 / \partial \Delta^2$ as a function of Δ for fixed $\delta = 0.3$ with different sizes N . (b) The extrapolation of the pseudo-critical points Δ^* . It is obtained $\Delta_c \approx 3.623$ with the exponent $\nu \approx 0.568$.

region $\Delta \lesssim 1$, and the correlation lengths are large. The typical DLC, as in Fig. 2(c), should only appear when the subsystem size is much larger than the correlation length. This makes numerical difficulty for finding the proper pseudo-critical point Δ_c^* . Therefore modifying the scanning route may also be considered, *i.e.* fixing Δ and varying δ . The precise ground-state phase diagram for the bond alternating XXZ model, shown in the Fig. 1(b), is determined by the above two methods and the scaling of the second derivatives of ground state energy density which is discussed below.

According to Ehrenfest's classification of phase transitions, the n th order quantum phase transition presents non-analyticity of the n th derivatives of ground state energy density at the critical point. It has been firstly shown that the 2nd derivative of ground state energy diverges at the 2nd order quantum critical point, but it remains a finite value for the 3rd and 5th order quantum phase transitions. [60] We report the results of energy derivatives for finding the critical points of the bond-alternating XXZ model Eq. (2). The ground state energy per site $e_0 = -\frac{1}{N} \sum_k R(k)$ for $\Delta = 0$ can be exactly obtained from Appendix A. In the thermodynamic limit $N \rightarrow \infty$, $e_0 = -\frac{4}{\pi} I(1 - \delta^2)$, where $I(x) = \int_0^{\frac{\pi}{2}} \sqrt{1 - x \sin^2 \theta} d\theta$ is the complete elliptic integral of the second kind. When $\delta = 0$, we have $e_0 = -\frac{\pi}{4}$, $\partial_\delta e_0 = 0$, and $\partial_\delta^2 e_0 \rightarrow -\infty$. Therefore, for the case $\Delta = 0$, the quantum phase transition at $\delta = 0$ belongs to second-order.

When $\Delta \neq 0$, by using DMRG, the 2nd derivative is calculated by the finite difference formula

$$\frac{\partial^2 e_0(g)}{\partial g^2} \approx \frac{e_0(g - \epsilon) - 2e_0(g) + e_0(g + \epsilon)}{\epsilon^2}. \quad (B1)$$

Where $e_0(g)$ is the ground state energy per site, g is the parameter of the Hamiltonian Eq. (2), and ϵ is taken to be 5×10^{-3} .

In absence of bond alternation, $\delta = 0$, it is known the system undergoes a Berezinskii-Kosterlitz-Thouless (BKT) quantum phase transition at the critical point $\Delta_c = 1$. [40] The BKT quantum phase transition is an infinite-order transition, and the n th derivative of energy diverges only if $n \rightarrow \infty$. However, the order of the transitions could be different and depend on the path in the phase diagram. It was first shown by Cross and Fisher [35] that the ground energy density of bond-alternating Heisenberg in proportion to $\delta^{4/3}$, and the 2nd derivatives of energy density $\partial_\delta^2 e_0 \propto \delta^{-2/3}$. Thus the 2nd

derivatives of energy density diverges and indicates a second order quantum phase transition at $\delta = 0$. On the other hand, for varying Δ and fixed $\delta = 0.3$, as shown in Fig. 9(a) and (b), the 2nd derivative of energy density diverges at the critical point $\Delta_c \approx 3.623$ in the thermodynamic limit $N \rightarrow \infty$. The values of the critical points obtained by the energy derivatives thus provide references for the values determined by the Rényi entropies S_2 and S_∞ . The precise phase diagram determined by the energy derivatives and the Rényi entropies is shown in the Fig. 1(b).

[1] Luigi Amico, Rosario Fazio, Andreas Osterloh, and Vlatko Vedral, “Entanglement in many-body systems,” *Rev. Mod. Phys.* **80**, 517–576 (2008).

[2] Ryszard Horodecki, Paweł Horodecki, Michał Horodecki, and Karol Horodecki, “Quantum entanglement,” *Rev. Mod. Phys.* **81**, 865–942 (2009).

[3] Otfried Gühne, Géza Tóth, and Hans J Briegel, “Multipartite entanglement in spin chains,” *New J. Phys.* **7**, 229 (2005).

[4] Christopher Eltschka, Thierry Bastin, Andreas Osterloh, and Jens Siewert, “Multipartite-entanglement monotones and polynomial invariants,” *Phys. Rev. A* **85**, 022301 (2012).

[5] Xiao-Gang Wen, “Topological order: From long-range entangled quantum matter to a unified origin of light and electrons,” *ISRN Condensed Matter Physics* **2013**, 198710 (2013).

[6] Simeng Yan, David A Huse, and Steven R White, “Spin-liquid ground state of the $s=1/2$ kagome heisenberg antiferromagnet,” *Science* **332**, 1173–1176 (2011).

[7] Xiao-Gang Wen, *Quantum Field Theory of Many-Body Systems:From the Origin of Sound to an Origin of Light and Electrons*, Oxford Graduate Texts (OUP Oxford, 2004).

[8] Charles H. Bennett, Herbert J. Bernstein, Sandu Popescu, and Benjamin Schumacher, “Concentrating partial entanglement by local operations,” *Phys. Rev. A* **53**, 2046–2052 (1996).

[9] Michael A. Nielsen and Isaac L. Chuang, *Quantum Computation and Quantum Information* (Cambridge University Press, 2000).

[10] Hui Li and F. D. M. Haldane, “Entanglement spectrum as a generalization of entanglement entropy: Identification of topological order in non-abelian fractional quantum hall effect states,” *Phys. Rev. Lett.* **101**, 010504 (2008).

[11] S. Turgut, “Catalytic transformations for bipartite pure states,” *J. Phys. A: Math. Theor.* **40**, 12185 (2007).

[12] M. Klimesh, “Inequalities that collectively completely...,” (2007), arXiv: 0709.3680.

[13] M. A. Nielsen, “Conditions for a class of entanglement transformations,” *Phys. Rev. Lett.* **83**, 436–439 (1999).

[14] Jian Cui, Mile Gu, Leong-Chuan Kwek, M. F. Santos, Heng Fan, and Vlatko Vedral, “Quantum phases with differing computational power,” *Nat. Commun.* **3**, 812 (2012).

[15] Si-Yuan Liu, Quan Quan, Jin-Jun Chen, Yu-Ran Zhang, Wen-Li Yang, and Heng Fan, “Phase diagram of quantum critical system via local...” (2015), arXiv: 1510.07115.

[16] Fabio Franchini, Jian Cui, Luigi Amico, Heng Fan, Mile Gu, Vladimir Korepin, Leong-Chuan Kwek, and Vlatko Vedral, “Local convertibility and the quantum simulation of edge states in many-body systems,” *Phys. Rev. X* **4**, 041028 (2014).

[17] Alioscia Hamma, Lukasz Cincio, Siddhartha Santra, Paolo Zanardi, and Luigi Amico, “Local response of topological order to an external perturbation,” *Phys. Rev. Lett.* **110**, 210602 (2013).

[18] Siddhartha Santra, Alioscia Hamma, Lukasz Cincio, Yigit Subasi, Paolo Zanardi, and Luigi Amico, “Local convertibility of the ground state of the perturbed toric code,” *Phys. Rev. B* **90**, 245128 (2014).

[19] Jian Cui, Luigi Amico, Heng Fan, Mile Gu, Alioscia Hamma, and Vlatko Vedral, “Local characterization of one-dimensional topologically ordered states,” *Phys. Rev. B* **88**, 125117 (2013).

[20] Xie Chen, Zheng-Cheng Gu, Zheng-Xin Liu, and Xiao-Gang Wen, “Symmetry-protected topological orders in interacting bosonic systems,” *Science* **338**, 1604–1606 (2012).

[21] Xie Chen, Zheng-Cheng Gu, Zheng-Xin Liu, and Xiao-Gang Wen, “Symmetry protected topological orders and the group cohomology of their symmetry group,” *Phys. Rev. B* **87**, 155114 (2013).

[22] Ian Affleck, Tom Kennedy, Elliott H. Lieb, and Hal Tasaki, “Rigorous results on valence-bond ground states in antiferromagnets,” *Phys. Rev. Lett.* **59**, 799–802 (1987).

[23] Pietro Smacchia, Luigi Amico, Paolo Facchi, Rosario Fazio, Giuseppe Florio, Saverio Pascazio, and Vlatko Vedral, “Statistical mechanics of the cluster ising model,” *Phys. Rev. A* **84**, 022304 (2011).

[24] W. Son, L. Amico, R. Fazio, A. Hamma, S. Pascazio, and V. Vedral, “Quantum phase transition between cluster and antiferromagnetic states,” *EPL (Europhysics Letters)* **95**, 50001 (2011).

[25] W. Son, L. Amico, and V. Vedral, “Topological order in 1d cluster state protected by symmetry,” *Quantum Information Processing* **11**, 1961–1968 (2011).

[26] Li Dai and Ming-Chiang Chung, “Breakdown of local convertibility through Majorana modes in a quantum quench,” *Phys. Rev. A* **91**, 062319 (2015).

[27] Helena Bragança, Eduardo Mascarenhas, G. I. Luiz, C. Duarte, R. G. Pereira, M. F. Santos, and M. C. O. Aguiar, “Nonuniversality of entanglement convertibility,”

Phys. Rev. B **89**, 235132 (2014).

[28] Yu-Chin Tzeng, “Parity quantum numbers in the density matrix renormalization group,” **Phys. Rev. B** **86**, 024403 (2012).

[29] Ingo Peschel, “Calculation of reduced density matrices from correlation functions,” **J. Phys. A: Math. Gen.** **36**, L205 (2003).

[30] Ming-Chiang Chung, Yi-Hao Jhu, Pochung Chen, and Chung-Yu Mou, “Quench dynamics of topological maximally entangled states,” **J. Phys.: Condens. Matter** **25**, 285601 (2013).

[31] Ling Qiang, Guang-Hua Liu, and Guang-Shan Tian, “Effects of bond alternation on the ground-state phase diagram of one-dimensional xxz model,” **Commun. Theor. Phys.** **60**, 240 (2013).

[32] L.-M. Duan, E. Demler, and M. D. Lukin, “Controlling spin exchange interactions of ultracold atoms in optical lattices,” **Phys. Rev. Lett.** **91**, 090402 (2003).

[33] Yu-Ao Chen, Sylvain Nascimbène, Monika Aidelsburger, Marcos Atala, Stefan Trotzky, and Immanuel Bloch, “Controlling correlated tunneling and superexchange interactions with ac-driven optical lattices,” **Phys. Rev. Lett.** **107**, 210405 (2011).

[34] S Korenblit, D Kafri, W C Campbell, R Islam, E E Edwards, Z-X Gong, G-D Lin, L-M Duan, J Kim, K Kim, and C Monroe, “Quantum simulation of spin models on an arbitrary lattice with trapped ions,” **New J. Phys.** **14**, 095024 (2012).

[35] M. C. Cross and Daniel S. Fisher, “A new theory of the spin-peierls transition with special relevance to the experiments on TTFCuBDT,” **Phys. Rev. B** **19**, 402–419 (1979).

[36] Kazuo Hida, “Crossover between the Haldane-gap phase and the dimer phase in the spin-1/2 alternating Heisenberg chain,” **Phys. Rev. B** **45**, 2207–2212 (1992).

[37] Masaaki Nakamura and Synge Todo, “Order parameter to characterize valence-bond-solid states in quantum spin chains,” **Phys. Rev. Lett.** **89**, 077204 (2002).

[38] Hsiang-Hsuan Hung and Chang-De Gong, “Numerical evidence of a spin-1/2 chain approaching a spin-1 chain,” **Phys. Rev. B** **71**, 054413 (2005).

[39] Liu Guang-Hua and Tian Guang-Shan, “Matrix product state, quantum entanglement, and criticality in the one-dimensional dimerized antiferromagnetic Heisenberg model,” **Comm. Theo. Phys.** **58**, 285 (2012).

[40] Thierry Giamarchi, *Quantum physics in one dimension* (Oxford University Press, 2003).

[41] W. P. Su, J. R. Schrieffer, and A. J. Heeger, “Solitons in polyacetylene,” **Phys. Rev. Lett.** **42**, 1698–1701 (1979).

[42] Shun-Qing Shen, *Topological Insulators: Dirac Equation in Condensed Matters*, Vol. 174 (Springer Science & Business Media, 2013).

[43] Steven R. White, “Density matrix formulation for quantum renormalization groups,” **Phys. Rev. Lett.** **69**, 2863–2866 (1992).

[44] Chia-Min Chung, Lars Bonnes, Pochung Chen, and Andreas M. Läuchli, “Entanglement spectroscopy using quantum monte carlo,” **Phys. Rev. B** **89**, 195147 (2014).

[45] C. M. Herdman, Stephen Inglis, P.-N. Roy, R. G. Melko, and A. Del Maestro, “Path-integral monte carlo method for Rényi entanglement entropies,” **Phys. Rev. E** **90**, 013308 (2014).

[46] David J. Luitz, Xavier Plat, Nicolas Laflorencie, and Fabien Alet, “Improving entanglement and thermodynamic Rényi entropy measurements in quantum monte carlo,” **Phys. Rev. B** **90**, 125105 (2014).

[47] Anushya Chandran, M. Hermanns, N. Regnault, and B. Andrei Bernevig, “Bulk-edge correspondence in entanglement spectra,” **Phys. Rev. B** **84**, 205136 (2011).

[48] Xiao-Liang Qi, Hoshio Katsura, and Andreas W. W. Ludwig, “General relationship between the entanglement spectrum and the edge state spectrum of topological quantum states,” **Phys. Rev. Lett.** **108**, 196402 (2012).

[49] Wen-Wei Ho, Lukasz Cincio, Heidar Moradi, Davide Gaiotto, and Guifre Vidal, “Edge-entanglement spectrum correspondence in a nonchiral topological phase and kramers-wannier duality,” **Phys. Rev. B** **91**, 125119 (2015).

[50] Frank Pollmann, Ari M. Turner, Erez Berg, and Masaki Oshikawa, “Entanglement spectrum of a topological phase in one dimension,” **Phys. Rev. B** **81**, 064439 (2010).

[51] G. Vidal, J. I. Latorre, E. Rico, and A. Kitaev, “Entanglement in quantum critical phenomena,” **Phys. Rev. Lett.** **90**, 227902 (2003).

[52] V. E. Korepin, “Universality of entropy scaling in one dimensional gapless models,” **Phys. Rev. Lett.** **92**, 096402 (2004).

[53] J. L. Cardy, “Entanglement entropy in extended quantum systems,” **Euro. Phys. J. B** **64**, 321–326 (2008).

[54] Rajibul Islam, Ruichao Ma, Philipp M. Preiss, M. Eric Tai, Alexander Lukin, Matthew Rispoli, and Markus Greiner, “Measuring entanglement entropy in a quantum many-body system,” **Nature** **528**, 77–83 (2015).

[55] Siew-Ann Cheong and Christopher L. Henley, “Many-body density matrices for free fermions,” **Phys. Rev. B** **69**, 075111 (2004).

[56] Anushya Chandran, Vedika Khemani, and S. L. Sondhi, “How universal is the entanglement spectrum?” **Phys. Rev. Lett.** **113**, 060501 (2014).

[57] Pasquale Calabrese, Massimo Campostrini, Fabian Essler, and Bernard Nienhuis, “Parity effects in the scaling of block entanglement in gapless spin chains,” **Phys. Rev. Lett.** **104**, 095701 (2010).

[58] Artur K. Ekert, Carolina Moura Alves, Daniel K. L. Oi, Michał Horodecki, Paweł Horodecki, and L. C. Kwek, “Direct estimations of linear and nonlinear functionals of a quantum state,” **Phys. Rev. Lett.** **88**, 217901 (2002).

[59] Dmitry A. Abanin and Eugene Demler, “Measuring entanglement entropy of a generic many-body system with a quantum switch,” **Phys. Rev. Lett.** **109**, 020504 (2012).

[60] Yu-Chin Tzeng, Hsiang-Hsuan Hung, Yung-Chung Chen, and Min-Fong Yang, “Fidelity approach to Gaussian transitions,” **Phys. Rev. A** **77**, 062321 (2008).